Available online at www.sciencedirect.com
SCIENCE DIRECT®
International Journal of Heat and Mass Transfer 48 (2005) 2159–2171
International Journal of HEAT and MASS TRANSFER
www.elsevier.com/locate/ijhmt

Minimum pumping power fluid tree networks without a priori flow regime assumption

Louis Gosselin *

Département de génie mécanique, Université Laval, Québec, Que., Canada G1K 7P4

Received 22 July 2004; received in revised form 31 December 2004
Available online 9 March 2005

Abstract

In this paper we approach the optimization of fluid tree networks by relaxing the usual one-flow regime assumption. The pumping power requirement is minimized, under global volume constraint. Two types of constructal network geometries are investigated: (i) the fluid users are distributed uniformly on a surface and, (ii) the fluid users are located on the periphery of a disc-shaped area. In both cases, the flow regime in a given pipe of the network emerges as a result of pumping power minimization. It is shown that the individual users' consumption and number of users dictate the transition from one optimal flow regime configuration to another. Under certain circumstances, laminar and turbulent flow regimes are present simultaneously in different pipes of an optimized network. The occurrence of turbulence at a certain level of pipes in the optimal hierarchical networks always leads to turbulence in the higher levels of pipes. The paper provides designers with basic tools for the conceptual design of fluid networks.

Keywords: Tree networks; Dendritic; Constructal; Geometry optimization; Turbulence; Transition

1. Introduction

One fascinating feature of tree networks is that they are not only present in engineering—i.e. man-made—architectures (e.g., fluid [1–6] and power [7] supply, road networks [1,8], cooling systems [1,9–11], wireless networks [12], etc.). They also occur abundantly in natural flow systems (e.g., respiratory airways [1,13,14], vascularized tissues [1,15,16], river basins and deltas [1,17,18], rapid solidification [19], etc.). The profusion of dendrites in nature and engineering, as well as their apparent similarities, can be rationalized: tree shape is the result of global optimization, under global constraints [1].

In many of the networks mentioned above, what is transported and delivered by the network is a fluid (e.g., air, water, oil, blood). In that case, the pumping power requirement is a good measure of the cost for operating the network [2]. Our objective as network designers is to minimize this operating cost, which is a global parameter: the power dissipated in each pipe is accounted for. We also face global constraints, in particular in terms of volume available for the network.

In most of the previous works on fluid network optimization [1–6,13–16], a flow regime in the pipes of the network is assumed a priori, *before* the optimization is performed. For example, one may assume that in a particular network the fluid flow is laminar, and optimize

* Tel.: +418 656 7829; fax: +418 656 7415.
E-mail address: louis.gosselin@gmc.ulaval.ca

0017-9310/$ - see front matter © 2005 Elsevier Ltd. All rights reserved.
doi:10.1016/j.ijheatmasstransfer.2004.12.037

Nomenclature

a	cross-sectional area, m^2
f	friction factor
L	length, m
$\dot{m}$	mass flow rate, $kg\ s^{-1}$
N	number of fluid consumers
Re	Reynolds number
S	construct level
$\dot{W}$	pumping power, $J\ s^{-1}$

Greek symbols

μ	dynamic viscosity, $kg\ m^{-1}\ s^{-1}$
v	kinematic viscosity, $m^2\ s^{-1}$
ρ	density, $kg\ m^{-3}$

Superscripts

$\sim$	dimensionless parameters
l	laminar regime
t	turbulent regime

Subscripts

c	critical
e	pipe index
m	minimized
opt	optimal

the network accordingly. If the flow in the network turns out not to be laminar in the end (i.e. the flow is actually turbulent) the network is not performing optimally, which results in a larger operating cost [2]. This is why it is useful to optimize the network without any flow regime assumption. In other words, the flow regime in a given pipe of the network is now an optimization result rather than an assumption.

Another reason for pursuing this goal is that more than one flow regime may be present simultaneously in different pipes of the same network. For example, the flow in the smaller pipes of the network may be laminar and the one in the larger pipes turbulent. In that case, the one-flow regime assumption fails. In this paper, we relax the one-flow regime assumption: we describe how to construct an optimal fluid distribution network without any flow regime assumption. The flow regime in a given pipe emerges as a result of optimization.

2. Problem formulation

Given a set of points, one of which is a fluid source, we want to connect the points with pipes in order to transport a fluid from the source to the other points. Examples of such fluid distribution networks were listed above in Section 1. The method presented in this paper can be extended to the problem of connecting a set of points with more than one source. The location of the points is known, and so is the consumption—the fluid mass flow rate required at every point.

Our objective is to transport the fluid with minimal pumping power (electrical power consumption). Pumping power as a "cost" function has been used in previous work on fluid network optimization, and it has been showed that in general it is not equivalent to minimizing pressure drop [2]. In this paper, we neglect the junction losses, and we suppose that in each pipe the flow is fully developed. This means that the pipes under consideration are long pipes—the pipe diameter-to-length ratio is small. In that case, it is well known that the pumping power for driving a mass flow rate $\dot{m}$ in laminar regime is [20,21]

$$\dot{W} = \frac{8\pi v \dot{m}^2 L}{\rho a^2} \tag{1}$$

Similar expressions for turbulent flow can be found in the literature. For example, the following empirical relation for the friction factor is commonly used for a turbulent fully developed flow in a smooth pipe [20,21]:

$$f = 0.046\left(\frac{2\dot{m}}{\mu\pi^{1/2}a^{1/2}}\right)^{-1/5} \tag{2}$$

Eq. (2) leads to the subsequent pumping power:

$$\dot{W} = 0.006\frac{\mu^{1/5}\dot{m}^{14/5}L}{\rho^2 a^{12/5}} \tag{3}$$

Note that pumping power expressions for fully developed turbulent flow in rough pipes could also be considered. The method developed in this paper would apply, but the resulting optimal network will depend on the roughness of the walls. More importantly, the key conclusion will be the same: the flow regime in a pipe of the network will emerge as an optimization result, not an assumption.

The range of applicability of Eqs. (1) and (3) depends essentially on the Reynolds number (Re) in the pipe, which in terms of the mass flow rate and pipe cross-sectional area reads as

$$Re = \frac{2\dot{m}}{\pi\mu a^{1/2}} \tag{4}$$

When Re in a pipe is smaller than the critical Reynolds number (Re_c) the flow is laminar. On the other hand, the flow is turbulent when Re is larger than Re_c. The value

of the critical Reynolds number in circular cross-section pipe is $Re_c \sim 2300$ [20,21].

Two types of constraints are invoked. The first is the total volume of the pipe network,

$$V = \sum_e a_e L_e \tag{5}$$

The summation is over all the pipes of the network. Although other types of constraints can be invoked for acknowledging the finiteness of the network, network total volume constraint has been used with success in the past [1–6,16]. The second type of constraint is the law of mass conservation at each point. The fluid consumption at a given point equals the difference between the inlet and outlet mass flow rates at that point.

In conclusion the problem consists of finding the network geometry that minimizes the total pumping power, i.e. the summation of the power dissipated in each pipe. Using Eqs. (1) and (3), the total pumping power, in a dimensionless form, can be written as:

$$\widetilde{W} = \sum_{e\,\mathrm{lam}} \frac{\tilde{m}_e^2 \widetilde{L}_e}{\tilde{a}_e^2} + K \sum_{e\,\mathrm{turb}} \frac{\tilde{m}_e^{14/5} \widetilde{L}_e}{\tilde{a}_e^{12/5}} \tag{6}$$

where

$$\widetilde{W} = \frac{W}{8\pi\rho\nu^3/L_{\mathrm{ref}}} \qquad \tilde{m} = \frac{\dot{m}}{\rho\nu L_{\mathrm{ref}}} \tag{7}$$

$$\tilde{a} = \frac{a}{L_{\mathrm{ref}}^2} \qquad \widetilde{L} = \frac{L}{L_{\mathrm{ref}}} \qquad Re = \frac{2\tilde{m}}{\pi^{1/2}\tilde{a}} \tag{8}$$

Two summation terms are present on the right-hand side of Eq. (6): the first summation is over the pipes with laminar flow, and the second one is over the pipes with turbulent flow. The dimensionless constant K is approximately equal to 2×10^{-3}. The reference lengthscale L_{ref} used to non-dimensionalize the variables can be any lengthscale of interest for the problem treated. In dimensionless form, the volume constraint, Eq. (5), becomes

$$\widetilde{V} = \frac{V}{L_{\mathrm{ref}}^3} = \sum_e \tilde{a}_e \widetilde{L}_e \tag{9}$$

3. The importance of relaxing the one-flow regime assumption

To illustrate how and why we shall relax the one-flow regime assumption, we begin with a simple example. Consider the network of Fig. 1, which is an arrangement of two pipes in series. The first pipe has a cross-sectional area $\tilde{a}_1$ and carries a mass flow rate $2\tilde{m}_0$ from the point i to the point j. As for the second pipe, its cross-sectional area and mass flow rate are respectively $\tilde{a}_0$ and $\tilde{m}_0$. This means that each one of the two sinks (points j and k) has the same fluid consumption which is equal to $\tilde{m}_0$. The length of the two pipes is the same and is used as the reference lengthscale in the non-dimensionalization of the

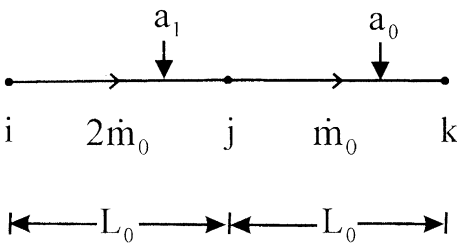

Fig. 1. The geometric configuration of a two-pipe network.

variables. To respect the fully developed flow assumption described in Section 2, the dimensionless volume of the pipe network has to be small, hence $\widetilde{V} \ll 1$. Because of the volume constraint, Eq. (9), only one of $\tilde{a}_0$ and $\tilde{a}_1$ can vary independently. We chose $\tilde{a}_0$ as the degree of freedom (DOF), which means that $\tilde{a}_1$ is obtained by Eq. (9): $\tilde{a}_1 = \widetilde{V} - \tilde{a}_0$.

Assuming that the flow in both pipes is laminar (case I), the total pumping power, Eq. (6), for this particular network becomes,

$$\widetilde{W}_I = \frac{4\tilde{m}_0^2}{\left(\widetilde{V} - \tilde{a}_0\right)^2} + \frac{\tilde{m}_0^2}{\tilde{a}_0^2} \tag{10}$$

which can be minimized with respect to $\tilde{a}_0$. The results of the optimization are $\tilde{a}_{0,\mathrm{opt}} = 0.3865\widetilde{V}$, $\tilde{a}_{1,\mathrm{opt}} = 0.6135\widetilde{V}$, $\widetilde{W}_{\mathrm{I,m}} = 17.32\tilde{m}_0^2\widetilde{V}^{-2}$. The assumption that the flow is laminar in both pipes holds if the largest Reynolds number in the network is smaller than the critical Reynolds number ($Re_c = 2300$). In this case, the largest Re is in the $\tilde{a}_1$-pipe and in view of Eq. (4), this Reynolds number is $Re = 2.88\tilde{m}_0\widetilde{V}^{-1/2}$. This means that the results presented in this paragraph (case I) are valid when $\tilde{m}_0 < 799\widetilde{V}^{1/2}$.

Similarly, assuming turbulent flow in the $\tilde{a}_1$- and $\tilde{a}_0$-pipes (case II), one finds: $\tilde{a}_{0,\mathrm{opt}} = 0.3610\widetilde{V}$, $\tilde{a}_{1,\mathrm{opt}} = 0.6390\widetilde{V}$, $\widetilde{W}_{\mathrm{II,m}} = 0.05749\tilde{m}_0^{14/5}\widetilde{V}^{-12/5}$. This result is valid only when the smallest Reynolds number in the network is larger than Re_c, i.e. when $\tilde{m}_0 > 1225\widetilde{V}^{1/2}$. Note that the optimal configuration ($\tilde{a}_{0,\mathrm{opt}}$, $\tilde{a}_{1,\mathrm{opt}}$) and performance ($\widetilde{W}_{\mathrm{m}}$) for case II are different than for case I.

There is a 'gap', where the one-flow regime assumption fails: when the flow is laminar in the small $\tilde{a}_0$-pipe and turbulent in the large $\tilde{a}_1$-pipe (case III). In view of the previous discussion, this happens when $799\widetilde{V}^{1/2} < \tilde{m}_0 < 1225\widetilde{V}^{1/2}$. In that case the total pumping power is

$$\widetilde{W}_{\mathrm{III}} = \frac{2^{14/5} K \tilde{m}_0^{14/5}}{\left(\widetilde{V} - \tilde{a}_0\right)^{12/5}} + \frac{\tilde{m}_0^2}{\tilde{a}_0^2} \tag{11}$$

The numerical minimization of Eq. (11) leads to the optimal $\tilde{a}_0$ shown in Fig. 2. The optimal geometry ($\tilde{a}_{0,\mathrm{opt}}$) is not a constant as in cases I and II, but varies with $\tilde{m}_0/\widetilde{V}^{1/2}$. The same is true for the optimal ratio $\tilde{a}_0/\tilde{a}_1$: it is a constant only when the flow is laminar

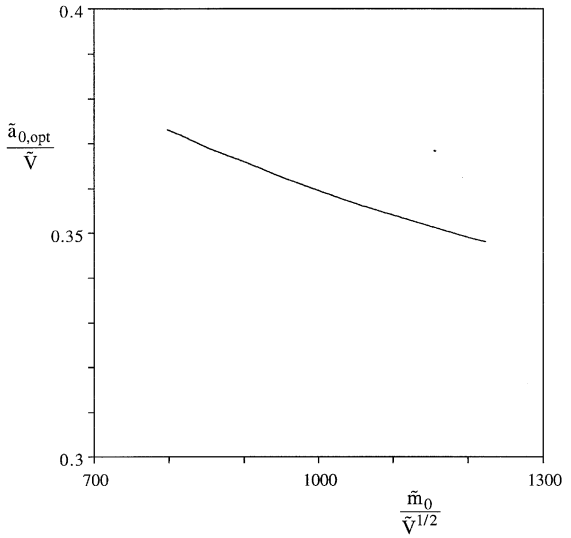

Fig. 2. The optimal $\tilde{a}_0$ for case III (turbulent regime in the first pipe, and laminar regime in the second pipe).

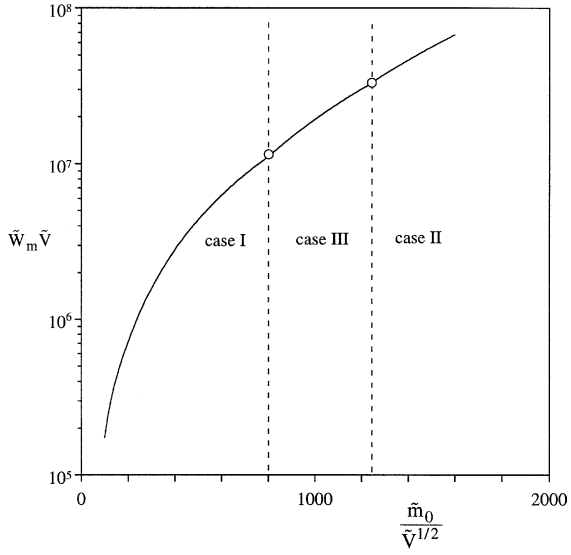

Fig. 3. The minimized pumping power as a function of the mass flow rate $\tilde{m}$.

($\tilde{a}_0/\tilde{a}_1 \sim 0.630$) or turbulent ($\tilde{a}_0/\tilde{a}_1 \sim 0.565$) in all the pipes. Otherwise, the optimal value of $\tilde{a}_0/\tilde{a}_1$ depends on $\tilde{m}_0/\widetilde{V}^{1/2}$. The minimized pumping power for the three possible flow regime configurations is shown in Fig. 3.

Fig. 4 shows what happens when the actual flow regime configuration in the network is different than the one that has been assumed for performing the optimization. Reported in the figure is the relative increase in terms of pumping power if the 'case I' or 'case II'-optimal architectures are used when the two-flow regime is

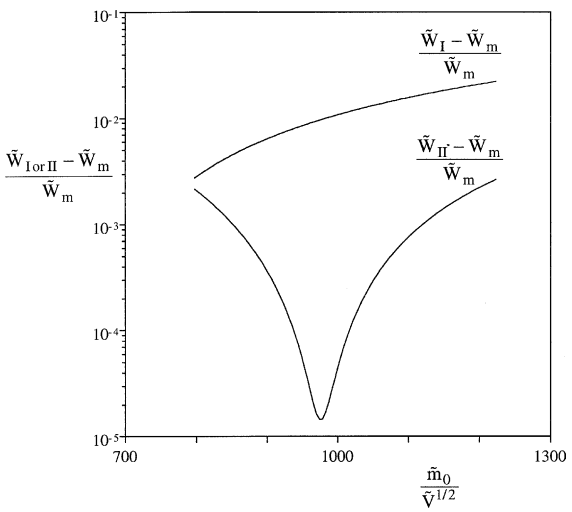

Fig. 4. The relative increase in pumping power when a network optimized for a given flow regime configuration is used under another flow regime configuration.

actually present (case III). The value of the power requirement increase depends strongly on the network under study (number, and position of the users, topology, etc.). Even though the relative increase is relatively weak in the present case (Fig. 4), a bad flow regime assumption can lead to much larger power requirement increase for more complex networks [2]. The key conclusion is that a wrong flow regime assumption results is a power requirement increase, which reinforces the importance of this paper. The flow regime in a given pipe of the network should be delivered by the optimization, not assumed. For the network of Fig. 1, the optimal flow regime configuration depends on the value of $\tilde{m}_0/\widetilde{V}^{1/2}$: when $\tilde{m}_0/\widetilde{V}^{1/2}$ is smaller than 799, the flow is laminar in both pipes (case I); when $\tilde{m}_0/\widetilde{V}^{1/2}$ is larger than 1225 the flow is turbulent in both pipes (case II); when $799 < \tilde{m}_0/\widetilde{V}^{1/2} < 1225$ the flow is turbulent in the first pipe, and laminar in the second pipe. This conclusion emerges as a result of optimization.

4. Constructal trees for fluid supply: elemental area

In the next sections, we generate a point-to-area fluid distribution network with the users uniformly distributed on the area [1]. All the users have the same fluid consumption $\tilde{m}_0$. We proceed from the smallest to the largest lengthscale, in line with the hierarchical optimization procedure described in Ref. [1] and called constructal design. From a construct level to the next one, the number of fluid consumers is doubled. The number of users can be increased until the whole area of interest is covered.

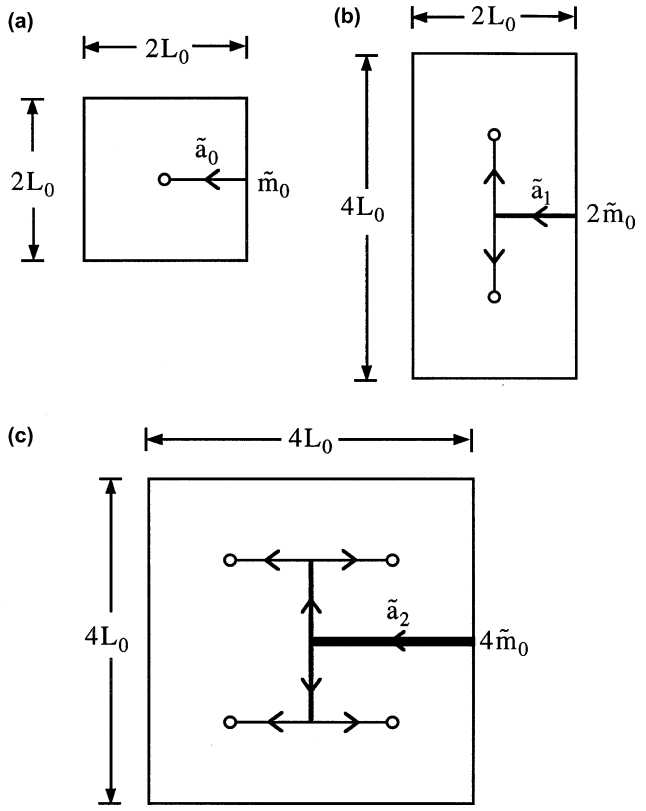

Fig. 5. The assembling of the constructal fluid tree: (a) the elemental area, (b) the first construct, and (c) the second construct.

We begin with the simple element shown in Fig. 5a. One fluid user located in the center of a square of size $2L_0$ is connected to the periphery with a pipe of length L_0. The dimensionless pumping power required to drive a laminar flow is

$$\widetilde{W}^{\mathrm{l}} = \frac{\tilde{m}_0^2}{\tilde{a}_0^2} \tag{12}$$

where we have used L_0 as the reference lengthscale. On the other hand, when the flow regime is turbulent in the pipe, the pumping power is

$$\widetilde{W}^{\mathrm{t}} = K\frac{\tilde{m}_0^{14/5}}{\tilde{a}_0^{12/5}} \tag{13}$$

In Eqs. (12) and (13), the superscripts l and t mean that the flow is respectively laminar or turbulent. We consider that the volume of the elemental network, Eq. (9), is fixed

$$\widetilde{V}_0 = \tilde{a}_0 \tag{14}$$

which leaves no degree of freedom to minimize the pumping power requirement at this level. To respect the fully developed flow assumption described in Section 2, the value of $\widetilde{V}_0$ has to be small, hence $\widetilde{V}_0 \ll 1$. The transition from the laminar to the turbulent regime happens when the Reynolds number is equal to the critical Reynolds number, that is at the following critical mass flow rate

$$\tilde{m}_{\mathrm{c},0} = \frac{\pi^{1/2} Re_{\mathrm{c}} \widetilde{V}_0^{1/2}}{2} \tag{15}$$

The reader can verify that Eq. (15) is equivalent, in an order of magnitude sense, to intersecting Eqs. (12) and (13). The subscript c refers to the critical value, while the subscript 0 refers to the elemental (zeroth) level of construct.

5. First construct

More interesting in terms of optimization opportunities is the network shown in Fig. 5b, where two elemental areas are assembled to form a first construct. Two levels of pipes are now present. This means that four flow regime configurations are feasible. We refer to these possibilities as ll, tt, lt, and tl, where the first letter corresponds to the flow regime in the elemental pipes ($\tilde{a}_0$), and the second letter refers to the flow regime in the first construct pipe ($\tilde{a}_1$). With the help of Eq. (6), one can

write the pumping power requirement for each of the four possible flow regime configurations

$$\widetilde{W}^{\mathrm{ll}} = \frac{2\tilde{m}_0^2}{\widetilde{V}_0^2} + \frac{4\tilde{m}_0^2}{(\widetilde{V}_1 - 2\widetilde{V}_0)^2} \tag{16}$$

$$\widetilde{W}^{\mathrm{tt}} = \frac{2K\tilde{m}_0^{14/5}}{\widetilde{V}_0^{12/5}} + \frac{2^{14/5}K\tilde{m}_0^{14/5}}{(\widetilde{V}_1 - 2\widetilde{V}_0)^{12/5}} \tag{17}$$

$$\widetilde{W}^{\mathrm{lt}} = \frac{2\tilde{m}_0^2}{\widetilde{V}_0^2} + \frac{2^{14/5}K\tilde{m}_0^{14/5}}{(\widetilde{V}_1 - 2\widetilde{V}_0)^{12/5}} \tag{18}$$

$$\widetilde{W}^{\mathrm{tl}} = \frac{2K\tilde{m}_0^{14/5}}{\widetilde{V}_0^{12/5}} + \frac{4\tilde{m}_0^2}{(\widetilde{V}_1 - 2\widetilde{V}_0)^2} \tag{19}$$

To write Eqs. (16)–(19), we invoked the finiteness of the pipe assembly total volume,

$$\widetilde{V}_1 = 2\widetilde{V}_0 + \tilde{a}_1 \tag{20}$$

where $\widetilde{V}_0 < \widetilde{V}_1 \ll 1$. For each flow regime configuration, one can minimize the pumping power requirement with respect to $\widetilde{V}_0/\widetilde{V}_1$. In other words, the designer must decide what portion of the total available volume for this first construct will serve the elemental channels, and what portion will serve the new pipe.

For the *ll*-configuration, the minimization of Eq. (16) yields

$$\widetilde{V}^{\mathrm{ll}}_{0,\mathrm{opt}} = \frac{\widetilde{V}_1}{2 + 2^{2/3}} \qquad \tilde{a}^{\mathrm{ll}}_{1,\mathrm{opt}} = \frac{2^{2/3}}{2 + 2^{2/3}}\widetilde{V}_1 \tag{21}$$

$$\widetilde{W}^{\mathrm{ll}}_{\mathrm{m}} = \frac{\tilde{m}_0^2}{\widetilde{V}_1^2}(2 + 2^{2/3})^3 \tag{22}$$

Eq. (21) is known as the Murray's law [16]. The optimization results of Eqs. (21) and (22) are valid only when the Reynolds number in the $\tilde{a}_1$-pipe is smaller than Re_c, which reads as

$$\tilde{m}_0 < \tilde{m}_{c,1} = \frac{\pi^{1/2} Re_c}{2^{5/3}(2 + 2^{2/3})^{1/2}} \widetilde{V}_1^{1/2} \tag{23}$$

We note the appearance of another critical mass flow rate that is different from the one derived in Section 4, Eq. (15). This new critical mass flow rate rules the appearance of turbulence in the first construct pipe, while Eq. (15) dictates the transition in the elemental pipes.

The minimization of Eq. (17) in the tt-limit is also straightforward. The results are:

$$\widetilde{V}^{\mathrm{tt}}_{0,\mathrm{opt}} = \frac{\widetilde{V}_1}{2 + 2^{14/17}} \qquad \tilde{a}^{\mathrm{tt}}_{1,\mathrm{opt}} = \frac{2^{14/17}}{2 + 2^{14/17}}\widetilde{V}_1 \tag{24}$$

$$\widetilde{W}^{\mathrm{tt}}_{\mathrm{m}} = \frac{K\tilde{m}_0^{14/5}}{\widetilde{V}_1^{12/5}}(2 + 2^{14/17})^{17/5} \tag{25}$$

The tt-flow regime configuration is valid when the Reynolds number in the $\tilde{a}_0$-pipe is larger than Re_c. This means that the critical mass flow rate is the same as in Eq. (15). The condition for Eqs. (24) and (25) to be valid is therefore:

$$\tilde{m}_0 > \tilde{m}_{c,0} = \frac{\pi^{1/2} Re_c}{2(2 + 2^{14/17})^{1/2}} \widetilde{V}_1^{1/2} \tag{26}$$

where we have replaced $\widetilde{V}_0$ in Eq. (15) by its optimal value, Eq. (24). Comparing Eqs. (23) and (26) we note that there is a gap between the ranges of applicability of the ll- and tt-configurations. This gap is where the two-regime configurations lie. We will show below that an optimal tl-network cannot actually exist. Therefore, the only optimal two-regime configuration possible for the network of Fig. 5b is when the flow is laminar in the $\tilde{a}_0$-pipes, and turbulent in the $\tilde{a}_1$-pipe (lt). The optimal lt-network is obtained by minimizing Eq. (18), which yields

$$(\widetilde{V}_1 - 2\widetilde{V}^{\mathrm{lt}}_{0,\mathrm{opt}})^{17/5} = \frac{2^{19/5}3K}{5}\tilde{m}_0^{4/5}(\widetilde{V}^{\mathrm{lt}}_{0,\mathrm{opt}})^3 \tag{27}$$

Eq. (27) can be solved numerically for obtaining $\widetilde{V}^{\mathrm{lt}}_{0,\mathrm{opt}}$ as a function of $\tilde{m}_0$. The result has been reported in Fig. 6. The curve has been plotted in the range $\tilde{m}_{c,0} > \tilde{m}_0 > \tilde{m}_{c,1}$, which is the range where the lt-regime is the optimal configuration. In Fig. 7, the minimized pumping power for the three possible flow regime configurations is shown. The two critical mass flow rate values, Eqs. (23) and (26), are indicated in the figure.

The only thing left is to prove that the tl-regime is not a minimum pumping power configuration. To do so, we take the derivative of Eq. (19) with respect to $\widetilde{V}_0$, set it equal to zero, and obtain

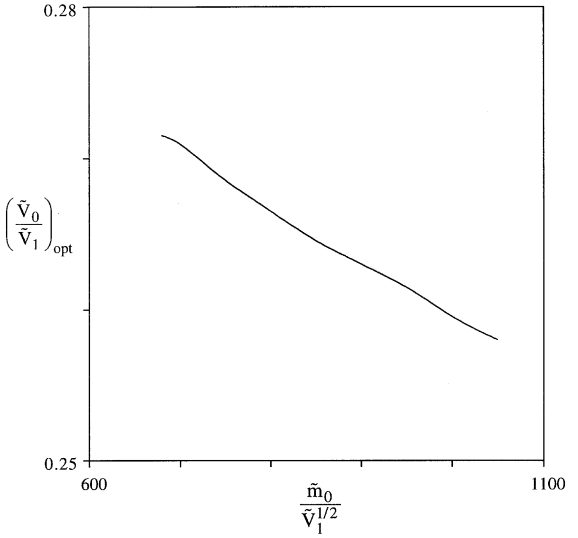

Fig. 6. The optimal $(\widetilde{V}_0/\widetilde{V}_1)^{\mathrm{lt}}_{\mathrm{opt}}$ as a function of $\tilde{m}_0$.

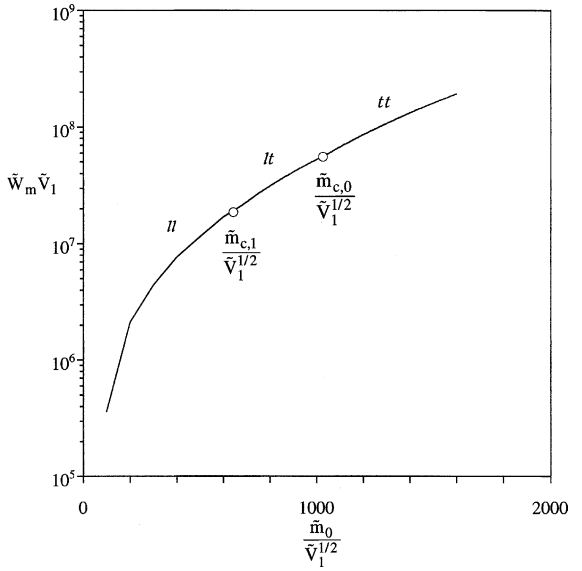

Fig. 7. The minimized pumping power in the first construct as a function of $\tilde{m}_0$.

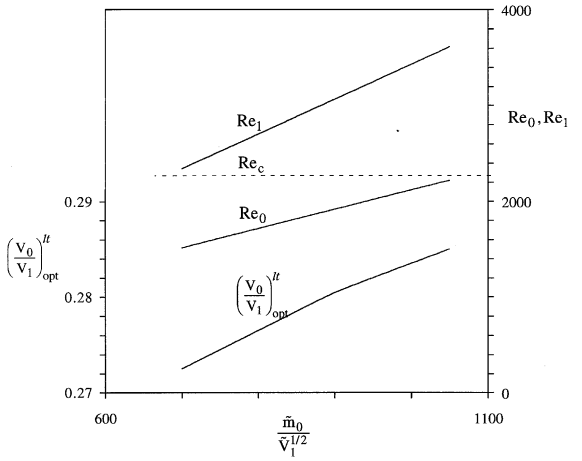

Fig. 8. The optimal $(\widetilde{V}_0/\widetilde{V}_1)^{tl}_{opt}$ as a function of $\tilde{m}_0$.

$$(\widetilde{V}_1 - 2\widetilde{V}^{tl}_{0,opt})^3 = \frac{10}{3K\tilde{m}_0^{4/5}}(\widetilde{V}^{tl}_{0,opt})^{17/5} \tag{28}$$

This equation has been solved numerically, and $\widetilde{V}^{tl}_{0,opt}$ is presented in Fig. 8. Also shown in Fig. 8 are the corresponding Reynolds numbers in the $\tilde{a}_0$- and $\tilde{a}_1$-pipes. One observes that these Reynolds numbers are actually incompatible with the assumptions of laminar flow in the $\tilde{a}_1$-pipe and turbulent flow in the $\tilde{a}_0$-pipe. In other words, the tl-regime is not an optimal flow regime configuration. Optimal networks exhibit laminar flow in the lower level pipes (smaller cross-sectional area), and turbulent flow in the higher level pipes (larger cross-sectional area).

6. Second and higher constructs

The second construct shown in Fig. 5c is an assembly of two first constructs connected with a new pipe, the cross-sectional area of which is $\tilde{a}_2$, in such a way that three levels of branching are present. Four flow regime configurations are to be expected: lll, llt, ltt, and ttt. We disregard the flow regime configurations where the flow is laminar in the larger pipes, and turbulent in the smaller ones for the reason described in Section 5. The total volume of the pipe network at this level is:

$$\widetilde{V}_2 = 2\widetilde{V}_1 + 2\tilde{a}_2 \tag{29}$$

The new DOF for the second construct is $\widetilde{V}_1/\widetilde{V}_2$, i.e. the amount of the total volume that is occupied by the pipes in the first construct. When the flow is laminar in all the pipes (lll), the pumping power requirement is

$$\widetilde{W}^{lll} = 2\widetilde{W}^{ll}_m + \frac{32\tilde{m}_0^2}{(\widetilde{V}_2/2 - \widetilde{V}_1)^2} \tag{30}$$

where $\widetilde{W}^{ll}_m$ is delivered by Eq. (22), and is a function of $\widetilde{V}_1$. The minimization of Eq. (30) leads to

$$\widetilde{V}^{lll}_{1,opt} = \frac{\widetilde{V}_2(2+2^{2/3})}{2^2+2^{5/3}+2^{7/3}}$$
$$\tilde{a}^{lll}_{2,opt} = \frac{2^{1/3}\widetilde{V}_2}{2+2^{2/3}+2^{4/3}} \tag{31}$$

$$\widetilde{W}^{lll}_m = \frac{\tilde{m}_0^2}{\widetilde{V}_2^2}(2^2+2^{5/3}+2^{7/3})^3 \tag{32}$$

Eqs. (31) and (32) are valid as long as the Reynolds number in the $\tilde{a}_2$-pipe is smaller than the critical Reynolds number, which means that the critical mass flow rate is

$$\tilde{m}_{c,2} = \frac{\pi^{1/2} Re_c \widetilde{V}_2^{1/2}}{2^{17/6}(2+2^{2/3}+2^{4/3})^{1/2}} \tag{33}$$

For the llt- and ltt-regime, the total pumping power requirement are respectively

$$\widetilde{W}^{llt} = 2\widetilde{W}^{ll}_m + K\frac{2^{33/5}\tilde{m}_0^{14/5}}{(\widetilde{V}_2/2 - \widetilde{V}_1)^{12/5}} \tag{34}$$

$$\widetilde{W}^{ltt} = 2\widetilde{W}^{lt}_m + K\frac{2^{33/5}\tilde{m}_0^{14/5}}{(\widetilde{V}_2/2 - \widetilde{V}_1)^{12/5}} \tag{35}$$

The results of the numerical minimization of Eqs. (34) and (35) are reported in Fig. 9. Finally, for the network in which the flow is turbulent in each pipe (ttt-regime), the optimization leads to

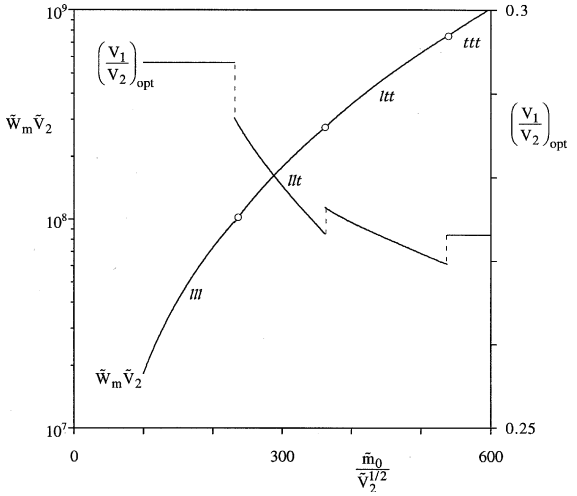

Fig. 9. The minimized pumping power and optimal $\widetilde{V}_1/\widetilde{V}_2$ for the second construct.

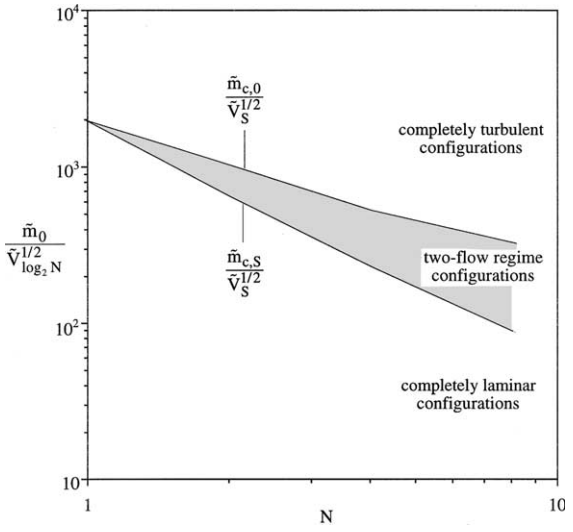

Fig. 10. The critical mass flow rate for the appearance of turbulence in the network as a function of the number of users when the users are distributed uniformly on an area.

$$\widetilde{V}_{1,\mathrm{opt}}^{\mathrm{ttt}} = \frac{\widetilde{V}_2(2+2^{14/17})}{2(2+2^{14/17}+2^{28/17})}$$

$$\tilde{a}_{2,\mathrm{opt}}^{\mathrm{ttt}} = \frac{2^{11/17}\widetilde{V}_2}{2+2^{14/17}+2^{28/17}} \tag{36}$$

$$\widetilde{W}_{\mathrm{m}}^{\mathrm{ttt}} = \frac{K\tilde{m}_0^{14/5}}{\widetilde{V}_2^{12/5}} 2^{17/5}(2+2^{14/5}+2^{28/5})^{17/5} \tag{37}$$

The minimum pumping power requirement is plotted in Fig. 9. The transitions from one flow regime configuration to another are indicated with small circles. The optimal $\widetilde{V}_{1,\mathrm{opt}}$ is also reported in Fig. 9 for the different flow regime configurations. The minimized pumping power requirement is a smooth function, which is not the case for the optimal $\widetilde{V}_1/\widetilde{V}_2$. At the transition from one flow regime configuration to another, one observes a discontinuity—a jump from one optimal architecture to another due to the flow regime changes within the network.

The procedure described above can be repeated for higher order constructs. At each level of construct, two lower level constructs are assembled, and connected with a new pipe. For the sake of conciseness, we do not repeat these steps here. Fig. 10 reports the evolution of the critical mass flow rate from one construct to another. S is the construct level, i.e. the number of levels of branching. Because of the doubling of the fluid users at each level, S is equal to $\log_2 N$, where N is the total number of fluid users. The upper curve in Fig. 10 corresponds to $\tilde{m}_{c,0}$, i.e. to the critical mass flow rate for the occurrence of turbulence at the elemental level. Therefore, all the points above that curve are such that the flow in the resulting network is turbulent in all the pipes. The bottom curve is for $\tilde{m}_{c,S}$, and dictates the occurrence of turbulence in the largest pipe of the network—the $\tilde{a}_S$-pipe. The flow is laminar in all the pipes of the network in the designs below that curve. The region between the two curves is where the optimal network exhibits a two-flow regime configuration. The optimal flow regime configuration can be read directly from Fig. 10. It is worth to note that the two-flow regime zone can actually be divided into sub-zones, because in general there may be more than one two-flow regime configuration. For example, when $S = 2$, the two two-flow regimes llt and ltt are present.

7. Fluid users distributed on the periphery of a disc-shaped area

Another benchmark problem for fluid network optimization [1–6] is when N fluid users are distributed uniformly on the periphery of a disc-shaped area, and the source is located at the center of the circle, Fig. 11. Each user has a fluid consumption equal to $\tilde{m}_0$. The problem is then to determine the optimal geometry (number of levels of branching, location of the branching points, etc.) when the flow regime configuration is unknown. The radius of the circle is used as the reference lengthscale to non-dimensionalize the variables, Eqs. (7) and (8).

When no pairing is present, as in Fig. 11a, there are N radial pipes with the same cross-sectional area $\tilde{a}_0$. Each pipe carries a mass flow rate $\tilde{m}_0$. The dimensionless length of the pipes is 1, because it is equal to the radius of the circle. The total pumping power requirement when the flow is laminar is,

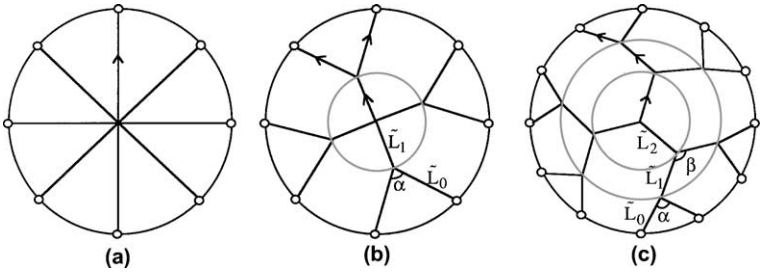

Fig. 11. The geometric features of a dendritic tree where the fluid users are distributed on the periphery of a circle: (a) radial pipes ($S = 0$), (b) one level of branching ($S = 1$), and (c) two levels of branching ($S = 2$).

$$\widetilde{W}^{1} = \frac{N\tilde{m}_0^2}{\tilde{a}_0^2} \tag{38}$$

However, because of the network volume constraint, $\widetilde{V} = N\tilde{a}_0$, we can rewrite Eq. (38) as

$$\widetilde{W}^{1} = \frac{N^3\tilde{m}_0^2}{\widetilde{V}^2} \tag{39}$$

Similarly, when the flow is turbulent the pumping power reads as

$$\widetilde{W}^{t} = \frac{KN^{17/5}\tilde{m}_0^{14/5}}{\widetilde{V}^{12/5}} \tag{40}$$

There is no optimization opportunity for the geometry shown in Fig. 11a. The pumping power requirement increases with N, and decreases with $\widetilde{V}$. The transition from laminar to turbulence flow occurs at the following critical mass flow rate which is a function of N

$$\tilde{m}_{c,0} = \frac{Re_c\pi^{1/2}\widetilde{V}^{1/2}}{2N^{1/2}} \tag{41}$$

8. One level of pairing

An optimization opportunity emerges in Fig. 11b, where the network exhibits one level of branching: there are $N/2$ outflows from the center that then split into N pipes to reach the N fluid users. The total pipe network volume is constrained, and is equal to

$$\widetilde{V} = N\tilde{a}_0\widetilde{L}_0 + \frac{N}{2}\tilde{a}_1\widetilde{L}_1 \tag{42}$$

The geometry of Fig. 11b is such that $\widetilde{L}_0$ and $\widetilde{L}_1$ can both be expressed as a function of α, the angle between two $\tilde{a}_0$-pipes,

$$\widetilde{L}_0 = \frac{\sin(\pi/N)}{\sin(\alpha/2)} \qquad \widetilde{L}_1 = \cos(\pi/N) - \frac{\sin(\pi/N)}{\tan(\alpha/2)} \tag{43}$$

There are thus only two parameters that can vary independently. We chose α and $\tilde{a}_0/\tilde{a}_1$ as the DOFs. For different values of N, we can minimize the pumping power requirement with respect to the two DOFs. This procedure is repeated for the three possible flow regime configurations: when the flow is laminar in both the $\tilde{a}_0$- and $\tilde{a}_1$-pipes (ll), when the flow is turbulent in all the pipes (tt), and when the flow is laminar in the $\tilde{a}_0$-pipes and turbulent in the $\tilde{a}_1$-pipes (lt). The details for the purely laminar and purely turbulent cases can be found elsewhere [1,2]. For the ll-configuration, the optimal parameters are

$$\alpha_{\text{opt}}^{\text{ll}} = 74.9346^\circ \qquad \left(\frac{\tilde{a}_0}{\tilde{a}_1}\right)_{\text{opt}}^{\text{ll}} = 2^{-2/3} \tag{44}$$

Those results are valid only for $N \geqslant 5$. Otherwise the optimal parameters correspond to the radial pipes of Section 7. Note that Eq. (44) corresponds to Murray's law [16]. The optimal parameters for the tt-regime are

$$\alpha_{\text{opt}}^{\text{tt}} = 55.5302^\circ \qquad \left(\frac{\tilde{a}_0}{\tilde{a}_1}\right)_{\text{opt}}^{\text{tt}} = 2^{-14/17} \tag{45}$$

for $N \geqslant 7$. For the two-flow regime configuration, the pumping power requirement is

$$\widetilde{W}^{\text{lt}} = \frac{N\tilde{m}_0^2\widetilde{L}_0}{\tilde{a}_0^2} + \frac{2^{9/5}KN\tilde{m}_0^{14/5}\widetilde{L}_1}{\tilde{a}_1^{12/5}} \tag{46}$$

which can be minimized numerically with respect to the two DOFs, $\tilde{a}_0/\tilde{a}_1$, and α. The optimal parameters and minimum pumping power are reported in Fig. 12. Important is that $(\tilde{a}_0/\tilde{a}_1)_{\text{opt}}^{\text{lt}}$ and $\alpha_{\text{opt}}^{\text{lt}}$ depend on $\tilde{m}_0/\widetilde{V}^{1/2}$, which was not the case in the ll- and tt-regimes, Eqs. (44) and (45).

The two critical mass flow rates are

$$\tilde{m}_{c,0} = \frac{\pi^{1/2}Re_c\widetilde{V}^{1/2}}{2^{31/34}N^{1/2}(\widetilde{L}_{1,\text{opt}}(N) + 2^{3/17}\widetilde{L}_{0,\text{opt}}(N))^{1/2}} \tag{47}$$

$$\tilde{m}_{c,1} = \frac{\pi^{1/2}Re_c\widetilde{V}^{1/2}}{2^{3/2}N^{1/2}(\widetilde{L}_{1,\text{opt}}(N) + 2^{1/3}\widetilde{L}_{0,\text{opt}}(N))^{1/2}} \tag{48}$$

When $\tilde{m}_0$ is smaller than $\tilde{m}_{c,1}$, the flow regime is laminar in both levels of pipes. On the other hand, when $\tilde{m}_0$ is larger than $\tilde{m}_{c,0}$, the flow regime is turbulent in both levels of pipes. Finally, when $\tilde{m}_0$ is between $\tilde{m}_{c,1}$ and $\tilde{m}_{c,0}$, the flow is laminar in the $\tilde{a}_0$-pipes and turbulent in the

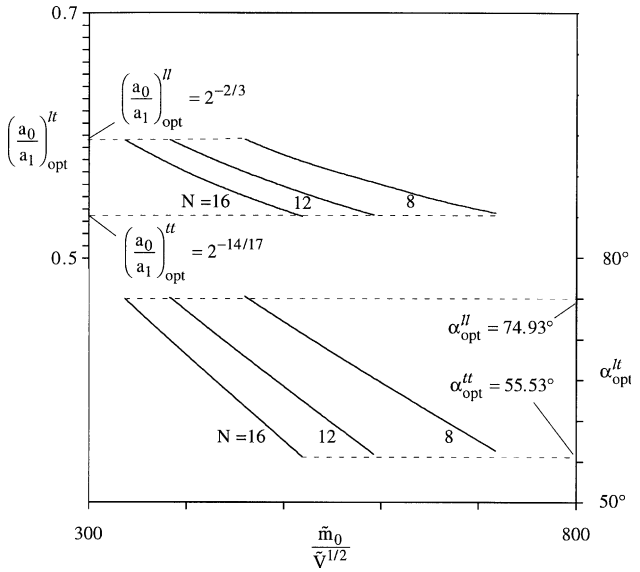

Fig. 12. The optimal α, and $\tilde{a}_0/\tilde{a}_1$ for the architecture of Fig. 11b.

$\tilde{a}_1$-pipes. Note that Eq. (47) is different than Eq. (40). In both cases though, the transition is a function of N.

9. Second and higher levels of pairing

It is possible to increase further the complexity of the dendrite by increasing the number of levels of branching, as in Fig. 11c where two levels of pairing are present. The total pipe volume is

$$\widetilde{V} = N\tilde{a}_0\widetilde{L}_0 + \frac{N}{2}\tilde{a}_1\widetilde{L}_1 + \frac{N}{4}\tilde{a}_2\widetilde{L}_2 \tag{49}$$

The lengths $\widetilde{L}_0$, $\widetilde{L}_1$, and $\widetilde{L}_2$ are function of the angles α and β,

$$\widetilde{L}_0 = \frac{\sin(\pi/N)}{\sin(\alpha/2)}$$

$$\widetilde{L}_1 = \frac{\sin(2\pi/N)}{\sin(\pi-\beta/2)}\left[\cos(\pi/N) - \frac{\sin(\pi/N)}{\tan(\alpha/2)}\right] \tag{50}$$

$$\widetilde{L}_2 = \frac{\sin(2\pi/N+\beta/2)}{\sin(\pi-\beta/2)}\left[\cos(\pi/N) - \frac{\sin(\pi/N)}{\tan(\alpha/2)}\right] \tag{51}$$

There are four parameters that can vary independently. We chose $\alpha, \beta, \tilde{a}_0/\tilde{a}_1$ and $\tilde{a}_1/\tilde{a}_2$ as the DOFs. For different values of N, the pumping power requirement can be minimized with respect to the four DOFs. This procedure can be repeated for the four possible flow regime configurations: lll, llt, ltt, and ttt. The optimal parameters are shown in Fig. 13, for $N = 16$.

In Fig. 14, the minimized pumping power requirement obtained with the three architectures of Fig. 11 ($S = 0$, 1, and 2, where S is the number of pairing levels) is reported for $N = 16$. With that number of users, the optimal architecture is the one with $S = 2$ for every values of $\tilde{m}_0$. The optimal flow regime configurations are indicated in the figure. As the value of $\tilde{m}_0$ increases, the optimal flow regime configuration changes from lll, to llt, ltt, and finally ttt. The transitions for the other values of S are also indicated with small circles.

Fig. 15 illustrates the minimized pumping power requirement for the case of 12 users ($N = 12$). The results are reported for three numbers of branching levels ($S = 0$, 1, 2). Note that there is no ttt optimal network for $N = 12$. In other words, for high values of $\tilde{m}_0/\widetilde{V}^{1/2}$, the ttt-optimal dendrite reduces to a tt-configuration (only one level of pairing), which is why the curve for $S = 2$ in Fig. 15 is absent for high values of $\tilde{m}_0/\widetilde{V}^{1/2}$. The optimal number of branching (S_{opt}) changes with the mass flow rate. For small mass flow rates ($\tilde{m}_0/\widetilde{V}^{1/2} < 475$), the optimal network has two levels of pairing ($S_{opt} = 2$). For larger values of $\tilde{m}_0/\widetilde{V}^{1/2}$, the optimal value of S is 1. As the value of $\tilde{m}_0$ increases, the optimal flow regime configuration changes from lll, to llt, lt, and finally tt, as indicated in Fig. 15.

We reported in Fig. 16 the critical mass flow rates in the optimal network as a function of N. As in Fig. 10 for the network where the users are distributed uniformly on a surface, there is a zone in the 'design space' where the flow is laminar or turbulent in all of the pipes. There is also a zone in the 'design space' where the optimal network is such that the flow is laminar in the smaller pipes and turbulent in the larger pipes. This zone is shadowed in Fig. 16. The optimal complexity—i.e. the optimal value of S—is not only a function of the number of users as in Refs. [3,5,6,10]. The value of S_{opt} is now also a

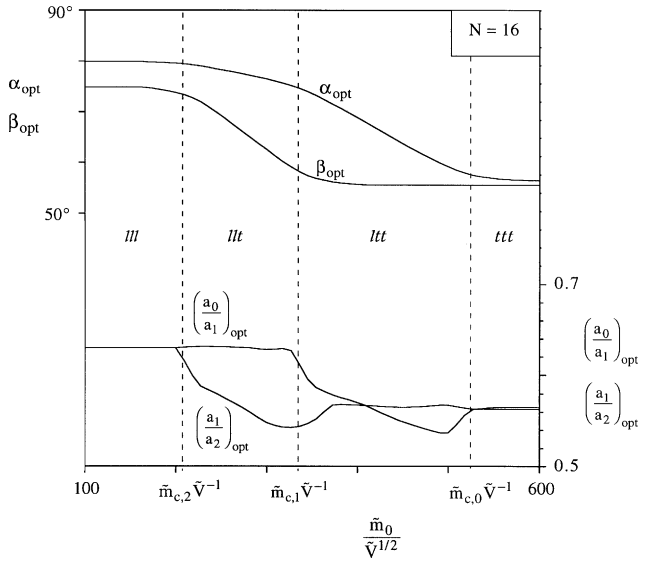

Fig. 13. The optimal α, β, $\tilde{a}_0/\tilde{a}_1$, and $\tilde{a}_1/\tilde{a}_2$ for the architecture of Fig. 11c.

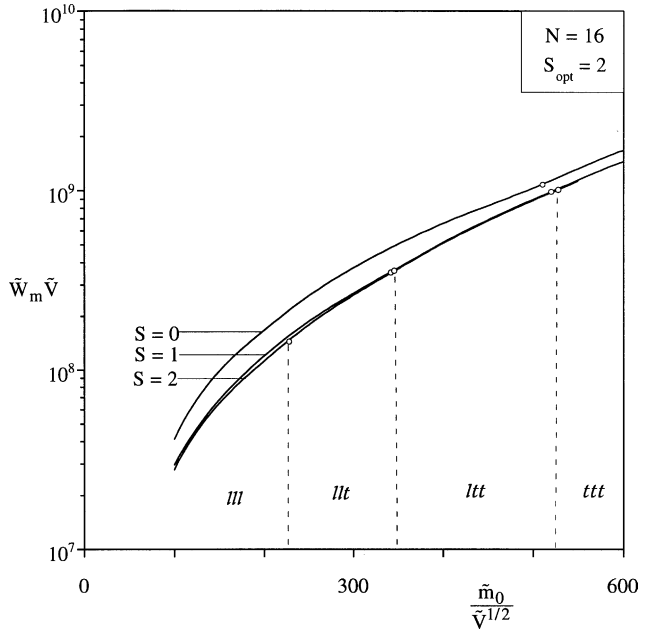

Fig. 14. The minimized pumping power requirement with the tree architectures of Fig. 11 ($S = 0$, 1, and 2) with 16 users.

function of the individual user consumption. The optimal flow regime configuration can be read directly from Fig. 16.

10. Concluding remarks

The pumping power requirement for a fluid distribution network is usually minimized on the basis of a flow regime assumption. In the present paper, we show that it is possible to relax that assumption is such a way that the flow regime in a given pipe of the network is a result of optimization. A new feature of the networks optimized with this approach is the possibility for both laminar and turbulent regimes to coexist in different pipes of the same network.

The approach has been applied to two types of constructal trees. The first one is a point-to-area network

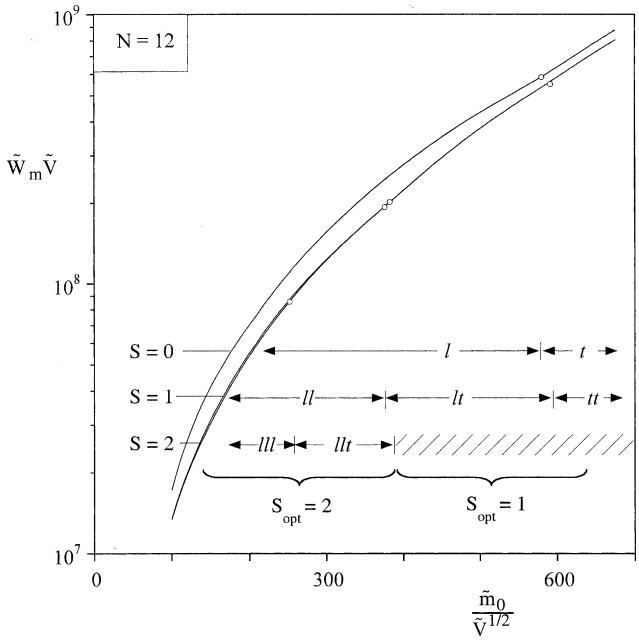

Fig. 15. The minimized pumping power requirement with the tree architectures of Fig. 11 ($S = 0$, 1, and 2) with 12 users.

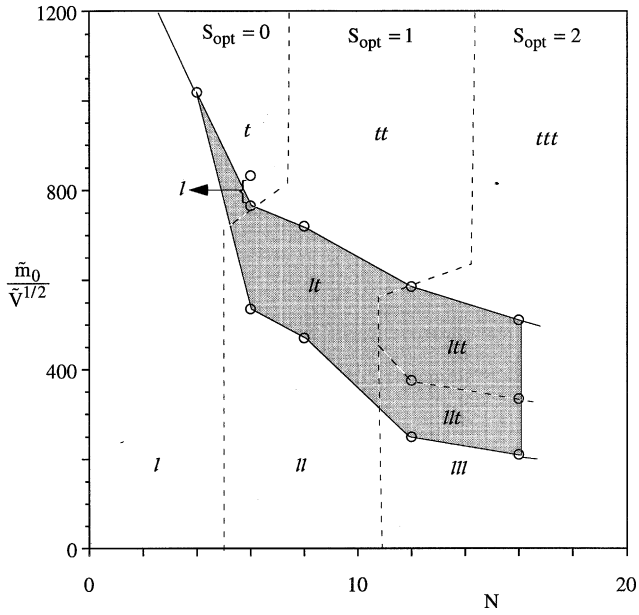

Fig. 16. The critical mass flow rate for the appearance of turbulence in the network as a function of the number of users when the users are located on the periphery of a disc-shaped area.

where the sinks are distributed uniformly on a surface. The second type of tree network is obtained when the sinks are distributed equidistantly on the periphery of a disc-shaped area, and the source is located in the center.

An important conclusion is that from one level of branching to another, the emergence of turbulence is a "point of no return". When turbulence appears at a certain level, the flow in the higher levels of branching will also be turbulent in the optimized constructal trees. This

statement is equivalent to the impossibility of finding an optimal tl-regime in Sections 5 and 8. The transition from laminar to turbulent regime in the network—i.e. the range of validity of the different flow regime configurations—is dictated by the total pipe volume constraint, number of users, and individual fluid users' consumption.

For the two problems considered, we showed that the flow is completely laminar or completely turbulent throughout the whole network only in certain zones of the 'design space', Figs. 10 and 16. There is also a zone where the flow regime configuration is a combination of laminar and turbulent regimes in different pipes of the network. We can draw an analogy with the growing of a boundary layer on a surface [20,21]: the two-flow regime zone (the gray zone in Figs. 10 and 16) is akin to the transition zone in the boundary layer, where the flow is not completely laminar, and not completely turbulent. A "transition zone" in the network emerges from the minimization of the dissipated power principle even though the turbulence model did not take into account the transition-regime in a single pipe.

It is also worth to point out the similarity between the results presented in this paper and the ones obtained in Ref. [9], where a heat-generating area was cooled with high thermal conductivity pathways. In Ref. [9], the transitions were between "bulk" and "nano" heat transfer regimes, depending on the thickness of the inserts.

The arranging of the distribution of flow leads to the construction of internal structure—optimal flow architecture for maximal global performance subject to constraints. The flow regime configuration in the network is an integral feature of the network structure, and therefore there is call for optimizing it.

References

[1] A. Bejan, Shape and Structure, from Engineering to Nature, Cambridge University Press, Cambridge, UK, 2000.
[2] L. Gosselin, A. Bejan, Tree network for minimal pumping power, Int. J. Thermal Sci. 44 (01) (2005) 53–63.
[3] S. Lorente, W. Wechsatol, A. Bejan, Optimization of tree-shaped flow distribution structure over a disc-shaped area, Int. J. Energy Res. 27 (2003) 715–723.
[4] N. Dan, A. Bejan, Constructal tree networks for the time-dependent discharge of a finite-size volume to one point, J. Appl. Phys. 84 (6) (1998) 3042–3050.
[5] S. Lorente, W. Wechsatol, A. Bejan, Tree-shaped flow structures designed by minimizing path lengths, Int. J. Heat Mass Transfer 45 (2002) 3299–3312.
[6] W. Wechsatol, S. Lorente, A. Bejan, Optimal tree-shaped networks for fluid flow in a disc-shaped body, Int. J. Heat Mass Transfer 45 (2002) 4911–4924.
[7] V. Arion, A. Cojocari, A. Bejan, Constructal tree shaped networks for the distribution of electrical power, Energy Convers. Manage. 44 (2003) 867–891.
[8] A. Bejan, Street network theory of organization in nature, J. Adv. Transport. 30 (1996) 85–107.
[9] L. Gosselin, A. Bejan, Constructal heat trees at micro and nanoscales, J. Appl. Phys. 96 (10) (2004) 5852–5859.
[10] W. Wechsatol, S. Lorente, A. Bejan, Dendritic heat convection on a disc, Int. J. Heat Mass Transfer 45 (2003) 4381–4391.
[11] L.A.O. Rocha, S. Lorente, A. Bejan, Constructal design of a cooling disc-shaped area by conduction, Int. J. Heat Mass Transfer 45 (2002) 1643–1652.
[12] S. Guthery, Wireless relay networks, IEEE Network 11 (6) (1997) 46–51.
[13] B. Mauroy, M. Filoche, E.R. Weibel, B. Sapoval, An optimal bronchial tree may be dangerous, Nature 427 (2004) 633–636.
[14] A.H. Reis, F. Miguel, M. Aydin, Constructal theory of flow architecture of the lungs, Med. Phys. 31 (2004) 1135–1140.
[15] K.L. Karau, G.S. Krenz, C.A. Dawson, Branching exponent heterogeneity and wall shear stress distribution in vascular trees, Am. J. Physiol.—Heart Circ. 280 (2001) H1256–H1263.
[16] C.D. Murray, The physiological principle of minimum work applied to the angle of branching of arteries, J. Gen. Physiol. 9 (1926) 835–841.
[17] J.D. Pelletier, D.L. Turcotte, Shapes of river networks and leaves: are they statistically similar? Philos. Trans. Royal Soc. Lond. Ser. B 355 (2000) 307–311.
[18] J.R. Banavar, F. Colaiori, A. Flammini, A. Maritan, A. Rinaldo, Scaling, optimality, and landscape evolution, J. Statist. Phys. 104 (2001) 1–48.
[19] C. Léger, J. Elezgaray, F. Argoul, Internal structure of dense electrodeposits, Phys. Rev. E 61 (2000) 5452–5463.
[20] A. Bejan, Convection Heat Transfer, second ed., Wiley, New York, 1995.
[21] F.M. White, Fluid Mechanics, fourth ed., McGraw-hill, Boston, 1999.